applied optics

# Ruling of echelles and gratings with a diamond tool by the torque equilibrium method

Jirigalantu,* Xiaotian Li, Shanwen Zhang, Xiaotao Mi, Jianxiang Gao, Bayanheshig, Xiangdong Qi, and Yuguo Tang

*Grating Technology Laboratory, Changchun Institute of Optics and Fine Mechanics and Physics, Chinese Academy of Sciences, Changchun, Jilin 130033, China*
**Corresponding author: jiri5998@163.com*

*Received 24 June 2016; revised 31 August 2016; accepted 31 August 2016; posted 7 September 2016 (Doc. ID 268912); published 30 September 2016*

**Ruling of echelles and gratings by the torque equilibrium method is proposed to eliminate corrugated grating lines, rough blazed grating surfaces, and complex fabrication work such as step-by-step diamond tool deflection. A mathematical model of the torque equilibrium between the diamond tool and the metallic film during the ruling process is deduced to realize optimized diamond tool geometrical parameter design. Then, two echelles with identical areas of 80 mm × 100 mm are separately ruled using the traditional deflecting tool ruling method and the proposed method, and the scatter light results for the two echelles are $9.6 \times 10^{-4}$ and $3.1 \times 10^{-4}$, respectively.** 

***OCIS codes:*** (050.1950) Diffraction gratings; (050.0050) Diffraction and gratings; (120.0120) Instrumentation, measurement, and metrology; (120.4640) Optical instruments.

http://dx.doi.org/10.1364/AO.55.008082

## 1. INTRODUCTION

Echelles and gratings, which are core components of large-scale, high-resolution optical spectrometers, large astronomical telescopes, and laser fusion systems, are widely used in various fields, including military, astronomy, new energy research, and biochemical analysis applications [1–9]. To date, the mechanical ruling method has been the primary production method used for large-area echelles and gratings [10–12]. Mechanical ruling is a process that involves diamond tool extrusion and polishing of the metal coating on the grating substrate and formation of stepped grooves on the metal coating [13], as shown in Fig. 1. The resulting grating grooves are finished using a combination of two perpendicular movements of the ruling engine: one in the ruling direction, and the other perpendicular to the ruling direction [14].

The largest grating ruling engines in the world are those of MIT-C in the United States [15–17], which can produce large echelles with dimensions of up to 450 mm × 635 mm. The new CIOMP-6 large grating ruling engine in China is now ready to be put into production to manufacture large gratings with dimensions of up to 400 mm × 500 mm [18]. While the history of mechanical grating ruling can be traced back for more than a century [14], the research has mainly focused on the design of the ruling system, the blank carriage system, and the interferometric control systems. However, the production of large gratings remains a challenging task because of the rather unclear mechanism that exists between the ruling tool and the grating film. Harrison's research on the ruling of large gratings and echelles using the MIT-C engine observed that eight of the ruled large gratings failed because of the unclear mechanism between the ruling tool and the film, and only four large gratings were successfully ruled from a total of 18 gratings [17]. The ruling tool is thus one of the most important factors in determining grating quality. Similar experiments have been performed in our laboratory on 79 gr/mm gratings with various dimensions, such as 160 mm × 250 mm and 400 mm × 500 mm, and we also found that the ruling tool and its working mode are very important for ruling of high-performance, large-area echelles and gratings.

However, the asymmetric cross section of the grating groove determines the asymmetry of the tool structure, and as a matter of course causes torque on the tool during the ruling process; this in turn strongly influences the groove linearity of the gratings and increases scatter light from these gratings. To reduce the influence of the tool torque on grating performance, a tool deflection method must be adopted before the formal grating ruling process, and this is a complex and time-consuming process because the tool direction must be deflected step-by-step according to the groove shape in each test. However, the tool deflection method cannot completely determine the torque equilibrium position of the ruling tool, and thus cannot completely eliminate the influence of tool torque on the grating

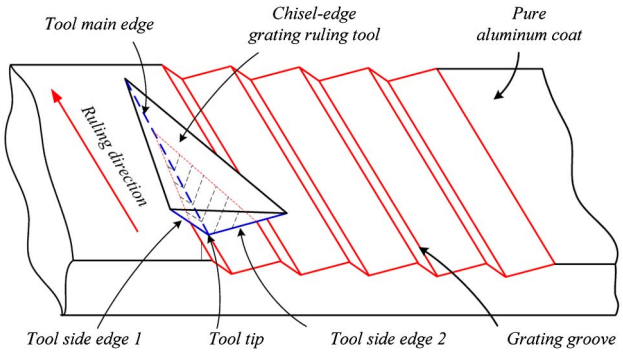


**Fig. 1.** Schematic view of chisel-edge ruling tool and grating ruling process.

performance; this leads to inconsistency between the ruling direction and the tool direction, which leads indirectly to transverse dissimilarity in the groove shape caused by enhanced tool wear, and finally causes greatly increased scatter light from the gratings.

To date, systematic studies of the extruded and polished forming mechanisms between the ruling tool and the grating films have rarely been performed. Therefore, in this paper, we propose a novel torque equilibrium method to be applied between the ruling tool and the grating films for ruling of echelles and gratings; the proposed method can eliminate corrugated grating lines, roughness in the blazed surfaces of gratings, and complex technical operations such as step-by-step deflection of the diamond tool. First, a mathematical model of the torque equilibrium during the ruling process is deduced to enable optimized design of the diamond tool geometrical parameters. Then, ruling experiments using both our method and the traditional tool deflection method with different deflection angles are performed, and the performance aspects of the gratings (such as the groove linearity and scatter light) produced by the two methods are compared.

Subsequently, two echelles with identical areas of 80 mm × 100 mm are separately ruled by the two methods. It is found that the proposed method does not require the time-consuming tool deflection processes, can obtain clean and smoothly ruled grooves in the gratings, and can achieve better scatter light levels, thus indicating the significance of our method for practical application to the ruling of large-area, high-performance echelles and gratings.

## 2. MATHEMATICAL TORQUE EQUILIBRIUM MODEL

The chisel-edge tool (also known as the double-ended or roof-edge tool) structure [13,14,19,20] is shown in Fig. 2; the cross section of the tool in the $Y$–$Z$ plane shows an asymmetrical "$V$" shape, and the main parameters of this tool include the tool side angle $D$, the tool side angle $F$, the back obliquity angle $H$, and the tool guide angle $\alpha$. The grating ruling direction, the names of the most important tool parts, and the tool's geometrical relationship with the coordinate axis are also shown in Fig. 2.

Figure 2 shows that the main edge is lifted slightly in the $X$–$Z$ plane to form an angle with the $X$ axis, called the pitching angle $E$, which is formed by the two side planes, called the $d$ plane and the $f$ plane. The two side edges are placed on the two side planes, called side edge 1 and side edge 2, which are formed by the intersection of the $d$ plane and the $f$ plane with the back obliquity plane. Additionally, the tool tip $O$ is at the intersection of the three planes and is placed on the $Z$ axis of the coordinate system.

Based on the specific triangular shape of the tool, the geometrical relationship between the tool parameters can easily be developed; for example, based on the triangular sine formula, we can obtain the relationship of side lengths to the angles on the $X$–$Y$ plane, as follows:

$$c/\sin(\lambda) = a/\sin(\alpha), \tag{1}$$

$$b/\sin(\beta) = a/\sin(\alpha). \tag{2}$$

The areas of the three tool planes are defined as $S_{\mathrm{ABO}} = S_H$, $S_{\mathrm{BCO}} = S_d$, and $S_{\mathrm{AOC}} = S_f$, and these planes are, respectively, expressed as

$$S_H = \frac{ch}{2\sin(H)}, \tag{3}$$

$$S_d = \frac{ah}{2\sin(D)}, \tag{4}$$

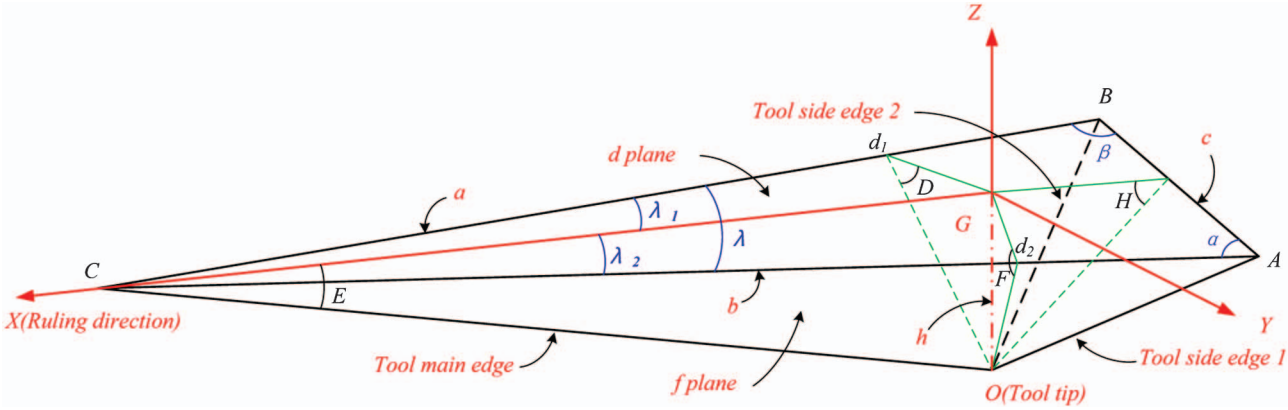


**Fig. 2.** Ruling tool structure and key tool parts with coordinate axes.

$$S_f = \frac{bh}{2\sin(F)}. \tag{5}$$

On the basis of the areas of these planes and the projection areas of these planes on the $X$–$Y$ plane, the relationship between the tool parameters and these areas can be developed in the form

$$\sqrt{p(p-a)(p-b)(p-c)} = S_d\cos(D) + S_f\cos(F) + S_H\cos(H), \tag{6}$$

where $p = \frac{1}{2}(a+b+c)$, $AB = c$, $BC = a$, and $AC = b$.

Based on the method shown in the above example, we can then develop relationships among all the tool parameters (the most important tool parameters are shown in Figs. 2 and 3), and the development of those relationships represents a good basis with which to perform a mechanical analysis of the tool.

When the chisel-edge tool is extruding and polishing the film, it must accept the resistance force of the film as part of the deformation process in the $X$-, $Y$-, and $Z$-axis directions. We define $pp_a$ as the normal pressure on the $d$ plane, and $tt_a$ as the shear pressure on the $d$ plane, with similar definitions for $pp_b$ and $tt_b$ on the $f$ plane. The included angles of the normal pressure $pp_a$ and the three coordinate axes are $x_a$, $y_a$, and $z_a$, as shown in Fig. 4. Using the same definitions, the normal and shear pressures on the $f$ plane can be expressed similarly using $x_b$, $y_b$, and $z_b$.

In the study of plowing and friction at the surfaces of plastic deformed metals by Liu *et al.*, they assumed that the normal pressure $p$ is approximately equal to the hardness $H_n$ of the plowed soft metal [21]. We can therefore assume that the normal pressure $pp$ on each plane of the ruling tool is also approximately equal to the film hardness $H_n$. Also, the shear pressure on each plane can be calculated based on the normal pressure $pp$ and the friction coefficient of 0.125.

Based on the developed triangular geometrical relationships among the tool parameters and the pressures on the tool on each side plane, we can develop a tool parametrical torque model centered on the $Z$ axis in the grating ruling process. By calculating the torque of each point on the projection area in the corresponding direction (i.e., $X$ or $Y$), we can then obtain the algebraic sum of the torques on the tool around the center of the $Z$ axis in the grating ruling process. For example, the total torque on the projection area $SCGO$ in the $Y$ direction is $N_{yaL}$. The total torque on a tool centered on the $Z$ axis is defined as $N$; the total torque produced in the $X$ direction is then defined as $N_x$, and the total torque produced in the $Y$ direction is defined as $N_y$, and these torques can be written as

$$N_{yaL} = \int_0^L (ppy_a - tty_a)(L-x)x\tan(E)\mathrm{d}x, \tag{7}$$

$$N_x = \frac{1}{6}((ttx_b + ppx_b)s_2^3\tan(B_2) - (ttx_a + ppx_a)s_1^3\tan(B_1)), \tag{8}$$

$$N_y = \frac{1}{6}(((ppy_a - tty_a)L_1^3\tan(A_1) + (ppy_b - tty_b)L^3\tan(E)) - ((ppy_b - tty_b)L_2^3\tan(A_2) + (ppy_a - tty_a)L^3\tan(E))), \tag{9}$$

$$N = N_x - N_y, \tag{10}$$

where $CG = L$, $GP3 = L1$, $GP4 = L2$, $Bp_3 = s_1$, and $Ap_4 = s_2$.

Because tool parameter $D$ is determined by the corresponding experimental data between the $D$ and the blaze angle of the different types of grating, our proposed torque model is indirectly dependent on blazed angle. For 79 gr/mm gratings with blaze angle of 63.4°, which is used in visible and infrared band applications, we can experimentally achieve this blaze angle by the tool with side angle of $D = 64°$.

Based on previous experience when ruling 79 gr/mm echelles, we can determine parts of these tool parameters, such as $D = 64°$, $F = 24°$, $\lambda = 4.5°$, and $h = 5.4$ μm, and based on the proposed tool torque model, we can draw curves of the total torque $N$ that are consistent with the tool guide angle and the back obliquity angle variation, as shown in Fig. 5.

The values of the tool torque $N$ centered around the $Z$ axis in the grating ruling process are shown in the form of a reduction curve and are transformed from positive to negative values with the variations in the tool guide angle. Both the guide angle and the back obliquity angle affect $N$ to the same extent, and the tool guide angle has a significant effect on the torque equilibrium point, as shown in Table 1.

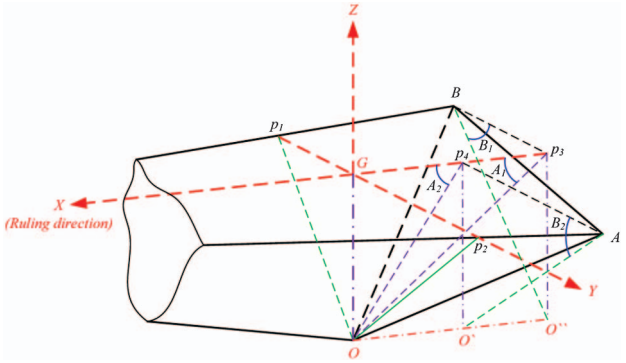


**Fig. 3.** Key ruling tool parameters with coordinate axes.

## 3. EXPERIMENTS AND DISCUSSION

For convenience when producing the tool, we selected the optimized grating ruling tool parameters with a guide angle of 2.3652 rad, and back obliquity angle of 10°, as shown in Table 1, and thus produced a tool with a guide angle of 2.4 rad and back obliquity angle of 10°. Additionally, we selected a traditional grating ruling tool with a guide angle of 0.5 rad and back obliquity angle of 19°. We then performed comparison experiments to assess the performance of the two different sets of tool parameters in terms of grating ruling quality. The ruling engine used in the experiments is CIOMP-2, and its tool support system consisted of two cross-hinge steel springs [11], as shown in Figs. 6 and 7.

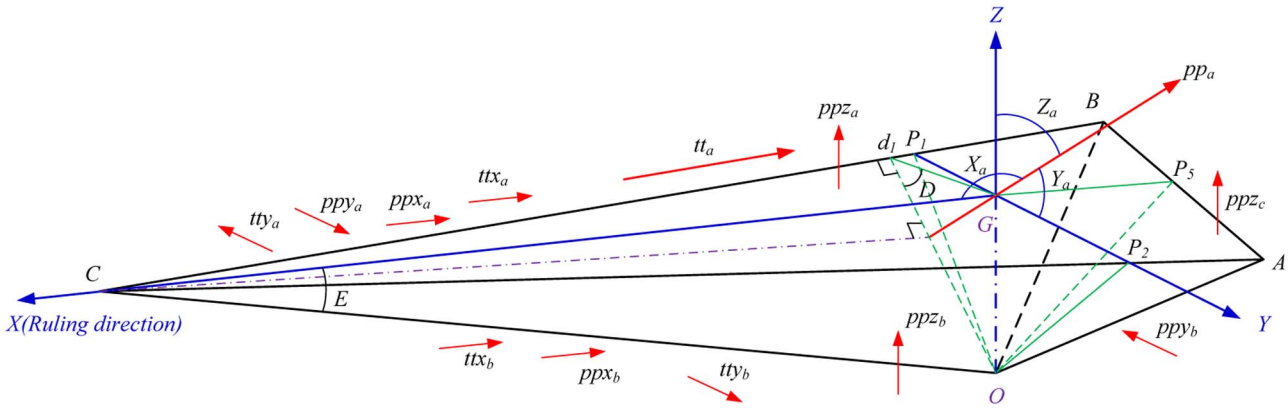


**Fig. 4.** Included angles of normal and shear pressure with coordinate axes.

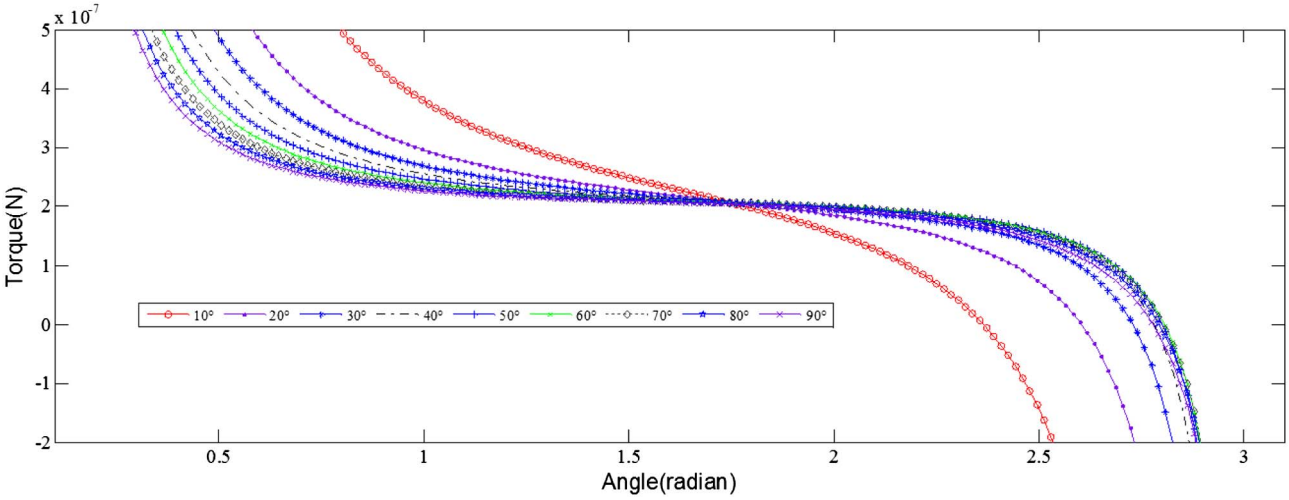


**Fig. 5.** Curves of $N$ consistent with the tool guide angle and the back obliquity angle variation.

The comparison experiments were carried out on a pure aluminum-coated quartz glass grating substrate with dimensions of 110 mm × 110 mm × 16 mm; the pure aluminum coating thickness was 10.5 μm, the thickness uniformity was less than 0.8%, and the surface roughness $Ra = 16$ nm. We then ruled the 79 gr/mm echelle with a blaze angle of 63.43° using both the traditionally designed tool and our optimized tool.

When the traditional tool is aligned correctly, the ruled groove lines show blurred and badly corrugated shapes; by deflecting the tool gradually to adjust the tool direction with respect to the ruling direction, we can eliminate the blurred and corrugated shapes to some extent via step-by-step adjustments, and finally determine the best tool working direction. As Fig. 8 (magnification of 5×) shows, the ruling sections of the gratings in panels (a), (b), (c), (d), and (e) correspond to tool deflection angles of 0°, 0.5°, 1°, 1.5°, and 2°, respectively, in the traditional ruling method, and we can clearly see the gradual variation of the grating grooves from corrugated lines to smooth lines. The corresponding groove linearity and shape for each of these ruling sections at a magnification of 50× are shown in Fig. 9. From the figure, we see that the ruled grating grooves are subject to corrugated lines and cutting effects when the traditional tool is aligned correctly; when the tool is deflected by 0.5°, the corrugated lines and cutting effects are still present, and when the tool is deflected to 1°, the corrugated lines disappear, although the cutting profile can still be clearly seen to some extent. Then, when the tool is deflected to 1.5°, the cutting profile becomes narrower, and, finally, when the tool is deflected to 2°, we obtain clean and smooth ruling grooves for the gratings.

**Table 1. Effect of Guide Angle and Back Obliquity Angle on Point at which $N = 0$**

| $H$ (°) | 10 | 20 | 30 | 40 | 50 | 60 | 70 | 80 | 90 |
|---|---|---|---|---|---|---|---|---|---|
| $\alpha$ (rad) | 2.3652 | 2.6047 | 2.7293 | 2.7815 | 2.8018 | 2.8071 | 2.8033 | 2.7938 | 2.7792 |

**Fig. 6.** CIOMP-2 grating ruling engine located in China.

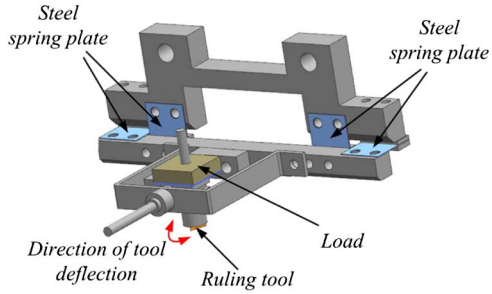


**Fig. 7.** Diamond support of CIOMP-2 grating ruling engine.

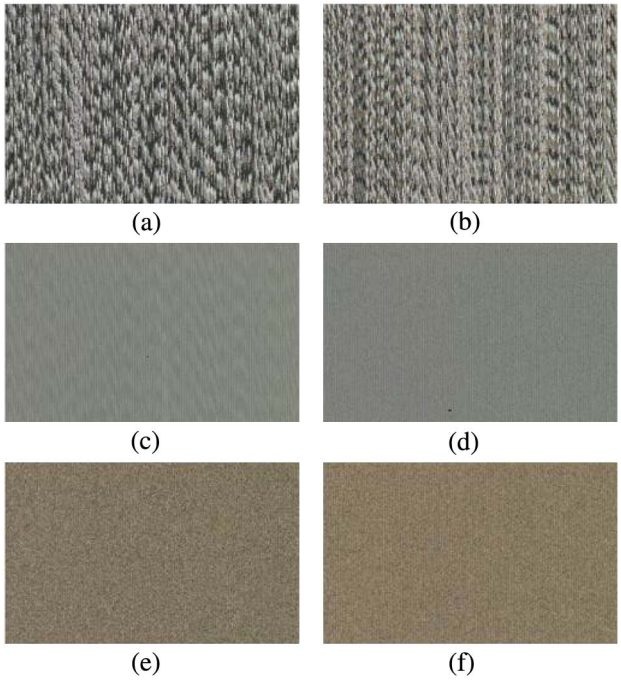


**Fig. 8.** Images of the ruling sections on the grating substrates, where (a)–(e) are ruled using a traditional tool with deflection angles of 0°, 0.5°, 1°, 1.5°, and 2°, respectively, and (f) is ruled using the proposed tool with a deflection angle of 0°.

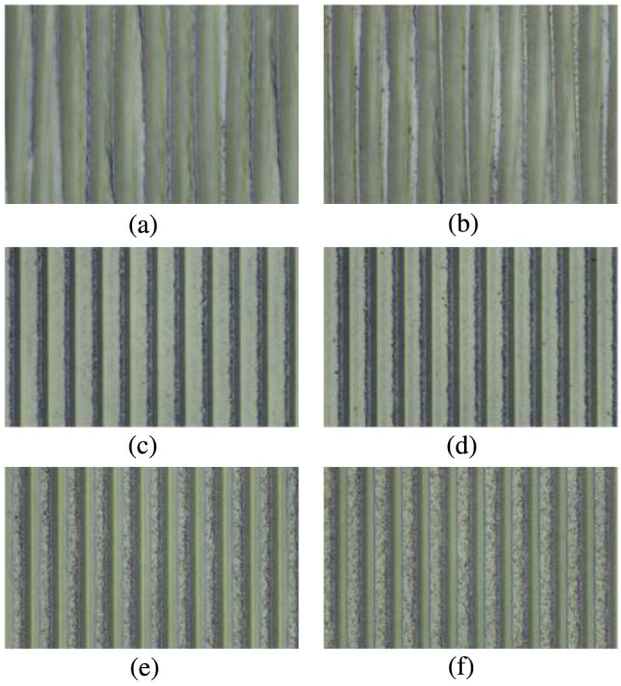


**Fig. 9.** Images of the groove linearity and shape for each ruling section on the grating substrates; (a)–(e) were ruled using a traditional tool with deflection angles of 0°, 0.5°, 1°, 1.5°, and 2°, respectively, while (f) was ruled using the proposed tool with a deflection angle of 0°.

The corresponding diffraction lines and spots of the grating at the 37th order in each of the ruling sections that were ruled using the traditional tool with different deflection angles and that ruled using the proposed tool are shown in Fig. 10. When the traditional tool is deflected over the range from 0° to 2°, the diffracted light from the corresponding ruled sections is gradually transformed from diffraction lines into spots. The diffracted light occurs as multiple lines on the ruled sections in Figs. 10(a) and 10(b), and then becomes spots on the ruled sections in Figs. 10(d) and 10(e). In addition, we can clearly see the slight differences in the diffracted light between Figs. 10(a), 10(b), and 10(c) that are produced by the corrugated groove lines; the cutting effects have little effect on groove linearity, but have a greater influence on the concentration of the diffraction spots.

When the proposed tool is aligned correctly, clean and smooth ruling grooves for the gratings are obtained directly, as shown in part (f) in both Figs. 8 and 9. The diffraction spots from this section of the grating at the 37th order are also clearly focused on single points, as shown in Fig. 10(f).

To ensure clear and comparable visual effects from the grooves on the gratings ruled using the tool at different deflection angles, we did not exert the full load on the diamond support. Based on these comparison experiments, we know that the groove linearity of the gratings that were ruled using the traditional tool with a deflection angle of 2° and by the proposed tool when correctly aligned is of similarly good quality. Therefore, we used the two different tools (traditional tool at the deflection angle of 2° and the proposed tool when correctly

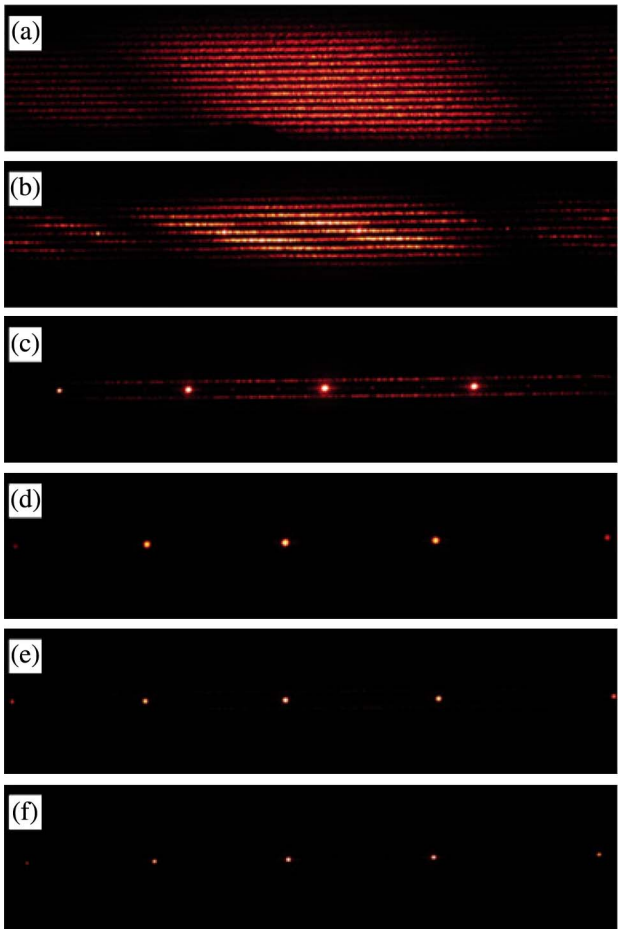


**Fig. 10.** Images of diffraction spots of grating at the 37th order in each of the ruling sections on the grating substrates, where (a)–(e) were ruled using the traditional tool with deflection angles of 0°, 0.5°, 1°, 1.5°, and 2°, respectively, and (f) was ruled using the proposed tool with a deflection angle of 0°.

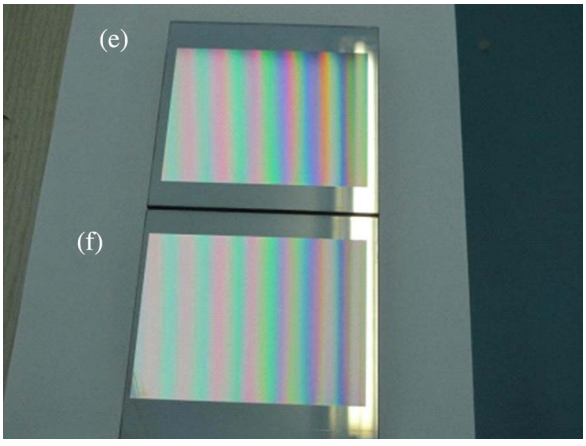


**Fig. 11.** Image of ruled formal gratings produced by a (e) traditional tool with deflection angle of 2° and (f) proposed tool when correctly aligned.

aligned) and exerted full loads on the diamond support to rule formal gratings with areas of 80 mm × 100 mm, as shown in Fig. 11. We then tested the scatter light of the two gratings when ruled using the two different tools. The measurement steps of scatter light are as follows: a 532 nm laser is irradiated to the grating surface, and the Thorlabs PM200 Energy Meter is used to measure the laser emitted light intensity ($I_0$) and the scatter light maximum value ($I_1$) between the 36th order and the 38th order; then, the value of grating stray light is $I_1/I_0$. Scatter light results of $9.6 \times 10^{-4}$ and $3.1 \times 10^{-4}$ are corresponding to the gratings ruled using the traditional tool with the deflection angle of 2° and our proposed tool, respectively.

From the formal ruling of the gratings using two different tools, we have shown that our tool can significantly improve both the groove linearity and the scatter light properties of the resulting echelles.

## 4. CONCLUSIONS

We propose a novel torque equilibrium method to be applied between the ruling tool and grating films for ruling of large-area echelles and gratings. Based on our method, we can provide the torque variation curve for the ruling tool with the variation of the guide angle and the back obliquity angle. The ruling tool can then be designed based on the torque curve. Comparison experiments were performed using the traditional tool deflection method and the proposed method, and the corresponding groove linearity and scatter light behavior of the gratings produced by the two methods are analyzed. Subsequently, two echelles with the same area of 80 mm × 100 mm were separately ruled by the two methods, and the scatter light results for the two echelles were determined to be $9.6 \times 10^{-4}$ and $3.1 \times 10^{-4}$, respectively.

It was found that our method can significantly improve the groove linearity and scatter light behavior of the resulting echelles and gratings. This illustrates the significance of the torque equilibrium method when applied between the ruling tool and the grating films for ruling of echelles and gratings, and can provide an important theoretical basis for the design of grating ruling tools. The proposed method is an effective way to solve the corrugated line and cutting effect problems on grating grooves, and can avoid the need for complex and time-consuming technical operations such as step-by-step tool deflection; this illustrates the significance of our method for practical applications in the ruling of large-area, high-performance echelles and gratings.

**Funding.** Chinese Finance Ministry for National R&D Projects for Key Scientific Instruments (ZDYZ2008-1); Ministry of National Science and Technology for National Key Basic Research Program of China (2014CB049500); Jilin provincial Science and Technology Development Program Project (20140204075GX); National Natural Science Foundation of China (NSFC) (61505204).

## REFERENCES

1. Z. Li, S. Li, C. Wang, Y. Xu, F. Wu, Y. Li, and Y. Leng, "Stable and near Fourier-transform-limit 30 fs pulse compression with a tiled grating compressor scheme," Opt. Express **23**, 33386–33395 (2015).
2. X. Wang, X. Wei, Y. Hu, X. Zeng, Y. Zuo, X. Hao, K. Zhou, N. Xie, and Y. Zhang, "Chirped-pulse amplification system based on chirp reversal and near-field spatial reversal with common tiled grating pair as stretcher and compressor," Appl. Opt. **51**, 5627–5632 (2012).

3. C. H. Chang, Y. Zhao, R. K. Heilmann, and M. L. Schattenburg, "Fabrication of 50 nm period gratings with multilevel interference lithography," Opt. Lett. **33**, 1572–1573 (2008).
4. C. Vannahme, M. Dufva, and A. Kristensen, "High frame rate multi-resonance imaging refractometry with distributed feedback dye laser sensor," Light Sci. Appl. **4**, e269 (2015).
5. J. Song, L. C. Chen, and B. J. Li, "A fast simulation method of silicon nanophotonic echelle gratings and its applications in the design of on-chip spectrometers," Prog. Electromagn. Res. **141**, 369–382 (2013).
6. J. Qiao, A. W. Schmid, L. J. Waxer, T. Nguyen, J. Bunkenburg, C. Kingsley, A. Kozlov, and D. Weiner, "*In situ* detection and analysis of laser-induced damage on a 1.5-m multilayer-dielectric grating compressor for high-energy, petawatt-class laser systems," Opt. Express **18**, 10423–10431 (2010).
7. N. Bonod and J. Neauport, "Diffraction gratings: from principles to applications in high-intensity lasers," Adv. Opt. Photon. **8**, 156–199 (2016).
8. Z. Li, T. Wang, G. Xu, D. Li, J. Yu, W. Ma, J. Zhu, L. Chen, and Y. Dai, "Research on potential problems of object image grating self-tiling for applications in large aperture optical systems," Appl. Opt. **52**, 718–725 (2013).
9. M. P. Wood and J. E. Lawler, "Aberration-corrected echelle spectrometer for measuring ultraviolet branching fractions of iron-group ions," Appl. Opt. **51**, 8407–8412 (2012).
10. G. R. Harrison, S. W. Thompson, H. Kazukonis, and J. R. Connell, "750-mm ruling engine producing large gratings and echelles," J. Opt. Soc. Am. **62**, 751–756 (1972).
11. X. T. Li, H. L. Yu, X. D. Qi, S. L. Feng, J. C. Cui, S. W. Zhang, Jirigalantu, and Y. Tang, "300 mm ruling engine producing gratings and echelles under interferometric control in China," Appl. Opt. **54**, 1819–1826 (2015).
12. Z. Li, J. Gao, H. Yang, T. Wang, and X. Wang, "Roughness reduction of large-area high-quality thick Al films for echelle gratings by multi-step deposition method," Opt. Express **23**, 23738–23747 (2015).
13. G. R. Harrison, "The production of diffraction gratings: II. The design of echelle gratings and spectrographs," J. Opt. Soc. Am. **39**, 522–528 (1949).
14. E. W. Palmer, M. C. Hutley, A. Franks, J. F. Verrill, and B. Gale, "Diffraction gratings," Rep. Prog. Phys. **38**, 975–1048 (1975).
15. G. R. Harrison, E. G. Loewen, and R. S. Wiley, "Echelle gratings: their testing and improvement," Appl. Opt. **15**, 971–976 (1976).
16. G. R. Harrison and S. W. Thompson, "Large diffraction gratings ruled on a commercial measuring machine controlled interferometrically," J. Opt. Soc. Am. **60**, 591–595 (1970).
17. G. R. Harrison, "The diffraction grating—an opinionated appraisal," Appl. Opt. **12**, 2039–2049 (1973).
18. C. Yang, X. Li, H. Yu, H. Yu, J. Zhu, S. Zhang, J. Gao, Bayanheshig, and Y. Tang, "Practical method study on correcting yaw error of 500 mm grating blank carriage in real time," Appl. Opt. **54**, 4084–4088 (2015).
19. D. A. Davies and G. M. Stiff, "Diffraction grating ruling in Australia," Appl. Opt. **8**, 1379–1384 (1969).
20. J. F. Verrill, "Diffraction grating ruling tool alignment by analysis of traced groove profile," J. Phys. E **8**, 522–525 (1975).
21. Z. Liu, J. Sun, and W. Shen, "Study of plowing and friction at the surfaces of plastic deformed metals," Tribol. Int. **35**, 511–522 (2002).